Journal of Structural Chemistry. Vol. 59, No. 7, pp. 1730-1736, 2018.
Original Russian Text © 2018 S. Taghavi Fardood, A. Ramazani, Z. Golfar, S. W. Joo.

GREEN SYNTHESIS USING TRAGACANTH GUM AND CHARACTERIZATION OF Ni–Cu–Zn FERRITE NANOPARTICLES AS A MAGNETICALLY SEPARABLE CATALYST FOR THE SYNTHESIS OF HEXABENZYLHEXAAZAISOWURTZITANE UNDER ULTRASONIC IRRADIATION

S. Taghavi Fardood[1], A. Ramazani[1,2], Z. Golfar[1], and S. W. Joo[3]

In this work, we report the synthesis, characterization, and catalytic evaluation of Ni–Cu–Zn ferrite using tragacanth gum as a biotemplate and metal nitrates as the metal source by the sol-gel method without using any organic chemicals. The sample is characterized by powder X-ray diffraction (XRD), Fourier transform infrared spectroscopy (FTIR), vibrating sample magnetometer (VSM), scanning electron microscopy (SEM), and energy dispersive X-ray analysis (EDX). The powder XRD analysis reveals the formation of cubic-phase ferrite MNPs with an average particle size of 20 nm. The magnetic analysis reveals that the Ni–Cu–Zn ferrite nanoparticles have ferromagnetic behavior at room temperature with a saturation magnetization of 52.76 emu/g. The catalytic activity of Ni–Cu–Zn ferrite MNPs is evaluated for the synthesis of 2,4,6,8,10,12-hexabenzyl-2,4,6,8,10,12-hexaazatetracyclo [5.5.0.05,9.03,11]dodecane (HBIW) under ultrasonic irradiation. Mild reaction conditions, short reaction times, the use of an economically convenient catalyst, and excellent product yields are the advantageous features of this method. The catalyst could be easily recycled and reused few times without a noticeable decrease in the catalytic activity.

DOI: 10.1134/S0022476618070296

Keywords: ferrite, tragacanth gum, natural gel, hexabenzylhexaazaisowurtzitane (HBIW), ultrasonic irradiation.

INTRODUCTION

Soft ferrites have been extensively used for many kinds of magnetic devices such as transformers, inductors, and magnetic heads for a high frequency because their electrical resistivity is higher than those of soft magnetic alloys. Various substitutions have been incorporated to achieve the desired electrical and magnetic properties [1-4]. Therefore, the synthesis of soft ferrites by a facile and green method is interesting. In general, ferrites belong to a large class of compounds having

---

[1]Department of Chemistry, University of Zanjan, Zanjan, Iran; saeidt64@gmail.com. [2]Research Institute of Modern Biological Techniques, University of Zanjan, Zanjan, Iran; aliramazani@gmail.com. [3]School of Mechanical Engineering, Yeungnam University, Gyeongsan, Republic of Korea; swjoo@yu.ac.kr. The text was submitted by the authors in English. *Zhurnal Strukturnoi Khimii*, Vol. 59, No. 7, pp. 1789-1795, September-October, 2018. Original article submitted November 9, 2017.

a spinel structure. Their physical properties are related to the structure of solids. The spinel unit cell consists of a cubic array of 32 oxygen anions, 16 Fe^{3+} ions, and 8 Fe^{2+} ions. A total of 24 metal cations are partitioned between eight tetrahedral and 16 octahedral interstices. In NiCuZn spinel ferrites, Zn^{2+} ions are known to prefer the occupation of tetrahedral (A) sites [5, 6] while Ni^{2+} and Cu^{2+} ions prefer the occupation of octahedral (B) sites, and Fe^{3+} ions partially occupy the A and B sites [5, 7].

Highly energetic compounds play an important role in the defense industry and other high-tech fields. In recent years, cage crystal molecules containing nitro groups have received great attention and are widely used as energetic materials [8, 9]. Hexanitrohexaazaisowurtzitane (HNIW or CL-20) with a wurtzitane ring system including nitramine, is the most prominent and relatively new powerful explosive in this class [10-12]. Hexabenzylhexaazaisowurtzitane (HBIW) is used as a precursor for the synthesis of HNIW. The condensation of glyoxal with benzylamine in the presence of formic acid as a catalyst is the only available method for constructing the HBIW cage [13, 14]. This method is efficient, but the catalyst could not be recovered and reused. Therefore, the introduction of efficient procedures with easily separable and reusable catalysts for the HBIW preparation is needed. For this purpose the use of magnetic catalysts such as Ni–Cu–Zn ferrite has received considerable attention. Its remarkable catalytic activity, easy synthesis, nontoxicity, reusability, economic viability, ecofriendliness, and recoverability encouraged us to utilize it as a catalyst for the HBIW synthesis.

Tragacanth gum (TG) is an acidic polysaccharide obtained from the bark of Astragalus gummifer (Fabaceae family), a native tree of Western Asia. Tragacanth gum is most commonly found in Iran [15, 16]. In the present study, we have synthesized Ni–Cu–Zn ferrite nanoparticles by Tragacanth gel without any surfactant. The catalytic activity of Ni–Cu–Zn ferrite nanoparticles has been evaluated for the HBIW synthesis with a facility and the appropriate method under eco-friendly conditions, as shown in Scheme 1.

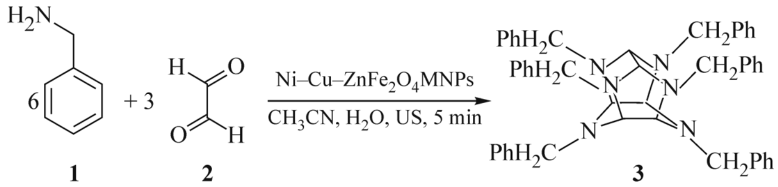

Scheme 1. HBIW synthesis in the presence of $NiCuZnFe_2O_4$ MNPs.

EXPERIMENTAL

Materials and techniques. Tragacanth gum (TG) was obtained from a local health food store. All the chemicals were purchased from Fluka AG, Merck, daijung (Darmstadt, Korea), Aldrich and were used without further purification. The reactions were monitored by TLC. Sonication was performed in Bandelin (Berlin, Germany) SONOPULS ultrasonic homogenizers with a 20 kHz processing frequency, a nominal power of 250 W, and uniform sonic waves. The melting point was measured with an Electrothermal 9100 apparatus (LABEQUIP LTD., Markham, Ontario, Canada) and was uncorrected. ^1H (DMSO-d_6) and ^{13}C NMR (DMSO-d_6) spectra were recorded on a Bruker DRX-250 Avance spectrometer at 250.13 MHz and 62.90 MHz, respectively.

The synthesized nanoparticles were characterized by four methods. Diffraction patterns and crystal structures of NPs were analyzed by XRD (X′Pert-PRO advanced diffractometer) at 40 kV with Cu(K_α) radiation (40 mA current, wavelength: 1.5406 Å) at room temperature in the 2θ range from 20° to 70°; the powder form of NPs was kept in sample tubs with double-sided tape to determine the structural morphology by SEM (Zeiss EVO 18) with an energy dispersive X-ray spectrometer (EDX) installed. The IR spectra were measured on a Jasco 6300 FT-IR spectrometer (KBr disks); the magnetic properties of sample were identified by vibrating sample magnetometer (VSM, Meghnatis Kavir Kashan Co., Kashan, Iran).

Methods. Preparation of $Ni_{0.35}Cu_{0.25}Zn_{0.4}Fe_2O_4$ MNPs. Firstly, 0.2 g of Tragacanth gum (TG) was dissolved in 40 ml of deionized water and stirred for 80 min at 70 °C to achieve a clear Tragacanth gel (TG) solution. Then, 0.35 mmol of $Ni(NO_3)_2\cdot6H_2O$, 0.25 mmol of $Cu(NO_3)_2\cdot6H_2O$, 0.4 mmol of $Zn(NO_3)_2\cdot6H_2O$, and 2 mmol of $Fe(NO_3)_3\cdot9H_2O$ were added to the TG solution. The reaction was performed at 75 °C in a sand bath with continuous stirring until the formation of brown resin. Finally, the powder was calcined at 700 °C for 4 h.

Typical procedure for the HBIW synthesis. Benzylamine (0.0085 mol, 0.937 ml), $NiCuZnFe_2O_4$ MNPs (7% mol with respect to glyoxal), acetonitrile (7.75 ml), and water (0.775 ml) were placed in a round-bottomed flask of 100 ml. The reaction mixture was stirred at room temperature and glyoxal (40% aqueous solution; 0.00375 mol, 0.427 ml) was added dropwise (15 min). Then the mixture was irradiated with ultrasound with a power of 150 W for 5 min. The HBIW formation was monitored by TLC. After the completion of the reaction, the reaction mixture was washed with excess cold ethanol and the catalyst was removed by a magnetic field. The precipitate was collected by simple paper filtration. For further purification acetonitrile was used. The reaction yield was 95% based on the obtained recrystallized product.

Spectral data. White solid; m.p.: 155-157 °C. FT-IR (KBr): 3022, 2942, 2835, 1951, 1601, 1450, 1351, 1169, 1138, 989, 926, 836, 732, 699. ^{1}HNMR ($CDCl_3$) δ_H: 7.24-7.28 (m, 30H, phenyl CH), 4.16 (s, 4H, CH_2), 409 (s, 8H, CH_2), 4.04 (s, 4H, CH), 3.57 (s, 2H, CH). ^{13}CNMR ($CDCl_3$): 56.21-56.88 (6C, CH_2-phenyl), 76.51-80.64 (6C, CH (skeletal), 126.62-140.74 (36C, phenyl).

RESULTS AND DISCUSSION

Catalyst characterization. The analysis of FT-IR spectra suggests two ranges of the absorption bands: in the range 400-1000 cm^{-1}, a metal–oxygen absorption band, typical of the spinel structure of ferrite, was observed at 580 cm^{-1} (Fig. 1). This band strongly suggests the intrinsic stretching vibrations of metal ($Fe \leftrightarrow O$) at the tetrahedral site. The bands at 3404 cm^{-1} and 1632 cm^{-1} are attributed to the hydroxyl group (O–H) vibrations. The peaks at 1456 cm^{-1} and 1017 cm^{-1} correspond to C–O and –C–O–C stretching modes [17].

The XRD pattern of as-synthesized $NiCuZnFe_2O_4$ prepared through the sol-gel method is shown in Fig. 2. It is seen from Fig. 2 that the XRD pattern consists of well-resolved peaks, which confirms the polycrystalline and monophasic nature of the prepared material.

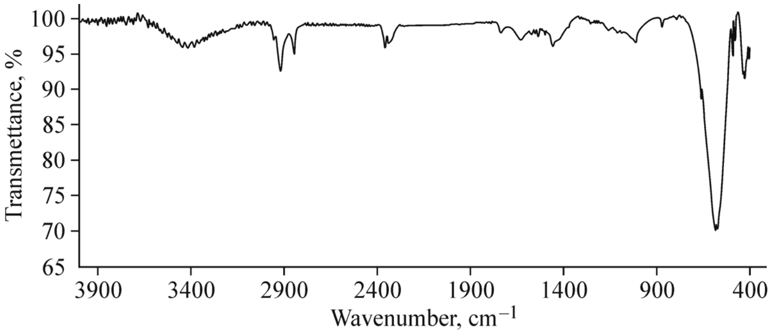

Fig. 1. FT-IR spectra of $Ni_{0.35}Cu_{0.25}Zn_{0.4}Fe_2O_4$ MNPs.

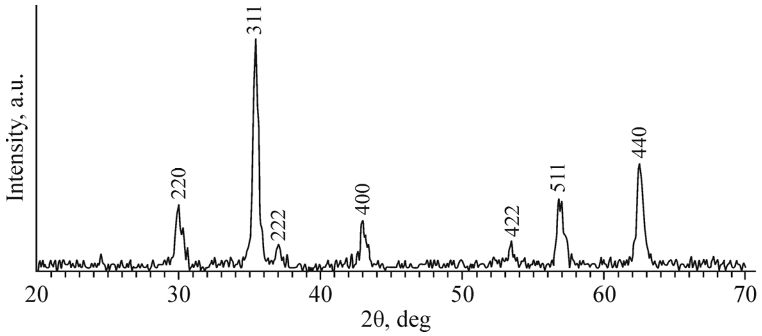

Fig. 2. XRD pattern of $Ni_{0.35}Cu_{0.25}Zn_{0.4}Fe_2O_4$ MNPs calcined in air at 700 °C for 4 h.

The identical XRD pattern of the sample exhibiting diffraction peaks at 2θ of 29.93, 35.36, 37.11, 43.01, 53.65, 56.83, and 62.51 corresponding to the (220), (311), (222), (400), (422), (511), and (440) planes of the crystal lattice, respectively, reveal their cubic structure, as found in the standard reference data (JCPDS Card no. 48-0489).

The average ferrite crystallite size can be calculated from the most intense (311) peak of the XRD pattern with the aid of the Scherrer formula

$$D = 0.9\lambda/\beta\cos\theta,$$

where D is the crystallite size; λ is the incident X-ray wavelength ($\mathrm{Cu}K_\alpha = 1.54$ Å); θ is the diffraction angle; β is the full width at half maximum (FWHM) of the most intense (311) diffraction peak [18]. We calculated an average crystallite size of 20 nm for the sample.

The SEM image of green synthesized $NiCuZnFe_2O_4$ MNPs is shown in Fig. 3. The morphology of synthesized MNPs identified the average size of 30-50 nm. The particles were clearly identified by their spherical shapes.

In order to study the magnetic behavior of $Ni_{0.35}Cu_{0.25}Zn_{0.4}Fe_2O_4$–NPs, magnetization measurements recorded with VSM were performed. The magnetization curve shows the ferromagnetic properties with magnetic remanence (M_r) and coercive force (H_c) being 80.14 Oe and 4.03 emu/g, respectively. As can be observed in Fig. 4, the specific saturation magnetization value was measured to be 52.76 emu/g for the sample.

EDX was performed to characterize the composition of the obtained nanoparticles. Fig. 5 demonstrates that $Ni_{0.35}Cu_{0.25}Zn_{0.4}Fe_2O_4$ MNPs obtained contains Ni, Cu, Zn, Fe, and O.

The role of the prepared catalyst in the HBIW synthesis was investigated under ultrasonic irradiation. We optimized the reaction conditions such as the catalyst amount, ultrasonic power, solvent type, and reaction times.

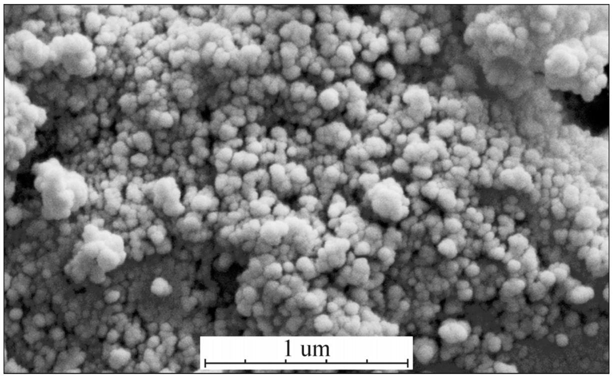

Fig. 3. SEM image of $Ni_{0.35}Cu_{0.25}Zn_{0.4}Fe_2O_4$ MNPs.

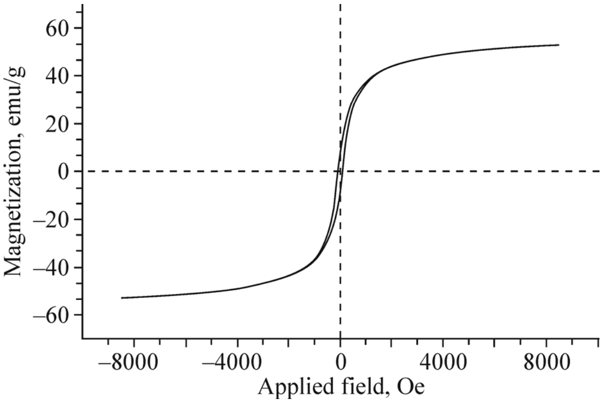

Fig. 4. Magnetization curve of $Ni_{0.35}Cu_{0.25}Zn_{0.4}Fe_2O_4$ MNPs.

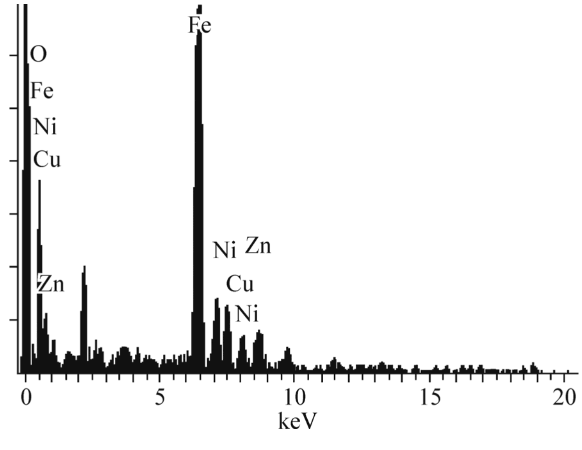

Fig. 5. EDX micrograph of $Ni_{0.35}Cu_{0.25}Zn_{0.4}Fe_2O_4$ MNPs.

Effect of the catalyst amount on the product yield. In order to verify the catalyst effect on the product yield, the reaction between benzylamine and glyoxal was carried out under different catalytic conditions. As shown in Table 1, when the reaction was carried out in the presence of Ni–Cu–$ZnFe_2O_4$ MNPs (7 mol% with respect to glyoxal), it led to the desired product in a 95% yield (Table 1, entry 4). In the absence of a catalyst, the reaction yielded only 14% of the product within 5 min (Table 1, entry 1).

Effect of various solvents on the product yield. We have investigated the effect of various solvents such as acetonitrile, chloroform, ethanol, methanol, and dichloromethane on the HBIW synthesis under ultrasound irradiation (5 min, 150 W). The results were summarized in Table 2. It is demonstrated that acetonitrile was the best choice for the model reaction.

Effect of the reaction time on the product yield. In order to optimize the reaction time, different reaction times selected for this study were 1 min, 3 min, 5 min, and 10 min. The effect of the reaction time on the HBIW performance was examined and the results are reported in Table 3.

Effect of the ultrasound power on the product yield. The effect of ultrasonic power inputs from 50 W to 200 W on the HBIW synthesis was evaluated (Table 4). The reaction yield increased with the ultrasonic power at 150 W in comparison to 50 W and 100 W but decreased at 200 W.

The catalytic activity and the ability to recycle and reuse of Ni–Cu–$ZnFe_2O_4$ MNPs were studied in this system. After the magnetic separation of the catalyst from the reaction mixture, the catalyst was washed with ethanol and dried to remove any remaining ethanol, and reused in the further reactions for several times. The average chemical yield for six consecutive runs was 89%, which clearly demonstrates the practical recyclability of this catalyst (Fig. 6).

A comparison of the catalytic efficiency of Ni–Cu–$ZnFe_2O_4$ MNPs with other catalysts for the HBIW synthesis is listed in Table 5. The result displays that this catalyst is superior to some other catalysts in terms of the magnetic separation, reusability, reaction time, and yield.

TABLE 1. Effect of the Catalyst in the HBIW Synthesis

Entry	Catalyst, mol%	Ultrasonic power, W	Time, min	Yield[a], %
1	None	150	5	14
2	3	150	5	67
3	5	150	5	90
4	7	150	5	95
5	10	150	5	95

Reaction conditions: benzylamine (0.0085 mol, 0.937 mL), glyoxal (0.0037 mol, 0.427 mL), CH_3CN (7.75 mL), H_2O (0.775 mL), and Ni–Cu–$ZnFe_2O_4$ MNPs (mol% with respect to glyoxal).

[a] Isolated yields.

TABLE 2. Synthesis of HBIW in the Presence of Ni–Cu–$ZnFe_2O_4$ MNPs in Different Solvents

Entry	Solvent	Yield[a], %
1	Acetonitrile	95
2	Chloroform	63
3	Ethanol	67
4	Methanol	78
5	Dichloromethane	58

Reaction conditions: benzylamine (0.0085 mol, 0.937 ml), glyoxal (0.0037 mol, 0.427 ml), solvent (7.75 ml), H_2O (0.775 ml), and Ni–Cu–$ZnFe_2O_4$ MNPs (7 mol% with respect to glyoxal).

[a] Yield of the product under ultrasound irradiation (5 min, 150 W).

TABLE 3. Different Runs for Choosing the Optimum Duration

Entry	Tim, min	Yield[a], %
1	1	41
2	3	78
3	5	95
4	10	95

Reaction conditions: benzylamine (0.0085 mol, 0.937 ml), glyoxal (0.0037 mol, 0.427 ml), acetonitrile (7.75 ml), H_2O (0.775 ml), and Ni–Cu–$ZnFe_2O_4$ MNPs (7 mol% with respect to glyoxal).

[a] Ultrasound irradiation (150 W).

TABLE 4. Effect of the Ultrasonic Irradiation Power on the HBIW Synthesis

Entry	Power, W	Time, min	Yield[a], %
1	50	5	62
2	100	5	86
3	150	5	95
4	200	5	93

Reaction conditions: benzylamine (0.0085 mol, 0.937 ml), glyoxal (0.0037 mol, 0.427 ml), acetonitrile (7.75 ml), H_2O (0.775 ml), and Ni–Cu–$ZnFe_2O_4$ MNPs (7 mol% with respect to glyoxal).

[a] Yield of the product.

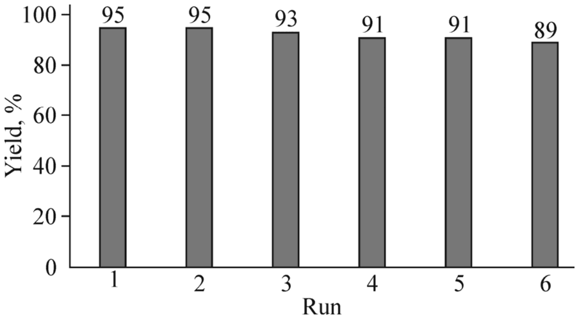

Fig. 6. Recyclability of $Ni_{0.35}Cu_{0.25}Zn_{0.4}Fe_2O_4$ MNPs.

TABLE 5. Comparison of the Catalytic Activity of Ni–Cu–$ZnFe_2O_4$ with Several Known Catalysts

Entry	Catalyst	Solvent	Conditions	Time, min	Yield[a], %	References
1	H_2SO_4	MeOH	60 °C	540	67	[19]
2	Chloric(VII) acid	Water/MeOH	50 °C	360	68	[20]
3	Citric acid	Water/acetonitrile	US	5	89	[21]
4	SiO_2 NPs	Water/acetonitrile	US	5	89	[8]
5	$CuFe_2O_4$ MNPs	Water/acetonitrile	US	16	89	[22]
6	Ni–Cu–$ZnFe_2O_4$ MNPs	Water/acetonitrile	US	5	95	[This work]

Reaction conditions: benzylamine (0.0085 mol, 0.937 ml), glyoxal (0.0037 mol, 0.427 ml), acetonitrile (7.75 ml), H_2O (0.775 ml), and Ni–Cu–$ZnFe_2O_4$ MNPs (7 mol% with respect to glyoxal).

[a] Yield of the product under ultrasound irradiation (5 min, 150 W).

CONCLUSIONS

In this study, we have reported the green synthesis of $Ni_{0.35}Cu_{0.25}Zn_{0.4}Fe_2O_4$ nanoparticles by the sol-gel method with tragacanth gel (TG) as a biopolymeric template. A single phase with a cubic spinel structure was formed after heat treatment at 700 °C for only 4 h. This method has many advantages such as nontoxicity, economic viability, easiness to scale up, less time consuming and environmentally friendly approach for the synthesis of Ni–Cu–Zn ferrite nanoparticles without using any organic chemicals. The catalytic activity of Ni–Cu–Zn ferrite nanoparticles has been evaluated for the HBIW synthesis under ultrasonic irradiation. The catalyst is inexpensive and easily available. Moreover, mild reaction conditions, simple procedure, short reaction times, easy workup, high yields of products, and easy separation and recyclability of the catalyst are the salient features of the presented work.

This work is funded by grant NRF-2018R1A2B3001246 of the National Research Foundation of Korea.

REFERENCES

1. G. Nabiyouni, H. Halakoui, and D. Ghanbari. *J. Nanostruct.*, **2016**, *7*, 77-81.
2. S. Taghavi Fardood, A. Ramazani, and S. Moradi. *J. Sol-Gel Sci. Technol.*, **2017**, *82*, 432-439.
3. K. Hedayati. *J. Nanostruct.*, **2015**, *5*, 13-16.
4. F. Sadri, A. Ramazani, H. Ahankar, S. Taghavi Fardood, P. Azimzadeh Asiabi, M. Khoobi, S. Woo Joo, and N. Dayyani. *J. Nanostruct.*, **2016**, *6*, 264-272.
5. A. El-Sayed. *Mater. Chem. Phys.*, **2003**, *82*, 583-587.
6. M. Ahmed, E. Ateia, L. Salah, and A. El-Gamal. *Mater. Chem. Phys.*, **2005**, *92*, 310-321.
7. M. Gabal. *J. Magn. Magn. Mater.*, **2009**, *321*, 3144-3148.
8. R. Arabian, A. Ramazani, B. Mohtat, V. Azizkhani, S. W. Joo, and M. Rouhani. *J. Energ. Mater.*, **2014**, *32*, 300-305.
9. P. Maksimowski, T. Gołofit, and W. Tomaszewski. *Cent. Eur. J. Energ. Mater.*, **2016**, *13*, 333-348.
10. A. T. Nielsen, A. P. Chafin, S. L. Christian, D. W. Moore, M. P. Nadler, R. A. Nissan, D. J. Vanderah, R. D. Gilardi, C. F. George, and J. L. Flippen-Anderson. *Tetrahedron*, **1998**, *54*, 11793-11812.
11. A. J. Bellamy. *Tetrahedron*, **1995**, *51*, 4711-4722.
12. Y. Bayat, H. Ebrahimi, and F. Fotouhi-Far. *Org. Process Res. Dev.*, **2012**, *16*, 1733-1738.
13. W. Qiu, S. Chen, and Y. Yu. *J. Chem. Crystallogr.*, **1998**, *28*, 593-596.
14. M. R. Crampton, J. Hamid, R. Millar, and G. Ferguson. *J. Chem. Soc., Perkin Trans.* **1993**, *2*(2), 923-929.
15. M. Zohuriaan and F. Shokrolahi. *Polym. Test.*, **2004**, *23*, 575-579.
16. N. Gralen and M. Kärrholm. *J. Colloid Sci.*, **1950**, *5*, 21-36.
17. R. Waldron. *Phys. Rev.*, **1955**, *99*, 1727-1735.
18. K. M. Batoo, S. Kumar, and C. G. Lee. *Curr. Appl Phys.*, **2009**, *9*, 826-832.
19. J. Jefimczyk, A. Antczak, and P. Maksimowski, *Przem. Chem.*, **2008**, *87*, 296-299.
20. T. Gołofit, P. Maksimowski, P. Szwarc, T. Cegłowski, and J. Jefimczyk. *Org. Process Res. Dev.*, **2017**, *21*, 987-991.
21. S. Shokrollahi, A. Ramazani, S. J. Tabatabaei Rezaei, A. Mashhadi Malekzadeh, P. Azimzadeh Asiabi, and S. W. Joo. *Iran. J. Catal.*, **2016**, *6*, 65-68.
22. V. Azizkhani, F. Montazeri, E. Molashahi, and A. Ramazani. *J. Energ. Mater.*, **2017**, *35*, 314-320.